

A massive galaxy that formed its stars at $z \sim 11$

Karl Glazebrook^{1*}, Themiya Nanayakkara¹, Corentin Schreiber²,
Claudia Lagos^{3,9,10}, Lalitwadee Kawinwanichakij¹, Colin Jacobs¹,
Harry Chittenden¹, Gabriel Brammer³, Glenn G. Kacprzak¹,
Ivo Labbe¹, Danilo Marchesini⁴, Z. Cemile Marsan⁵,
Pascal A. Oesch^{3,6}, Casey Papovich⁷, Rhea-Silvia Remus¹¹,
Kim-Vy H. Tran^{8,9}, James Esdaile¹, Angel Chandro-Gomez¹⁰

¹Centre for Astrophysics and Supercomputing, Swinburne University of Technology, P.O. Box 218, Hawthorn, 3122, VIC, Australia.

²IBEX Innovations, Sedgefield, Stockton-on-Tees, TS21 3FF, United Kingdom.

³Cosmic DAWN Center, Niels Bohr Institute, University of Copenhagen, Jagtvej 128, Copenhagen N, DK-2200, Denmark.

⁴Physics and Astronomy Department, Tufts University, 574 Boston Avenue, Medford, MA, 02155, USA.

⁵Department of Physics and Astronomy, York University, 4700 Keele Street, Toronto, ON, M3J 1P3, Canada.

⁶Department of Astronomy, University of Geneva, Chemin Pegasi 51, Versoix, CH-1290, Switzerland.

⁷Department of Physics and Astronomy, and George P. and Cynthia Woods Mitchell Institute for Fundamental Physics and Astronomy, Texas A&M University, College Station, TX 77843-4242, USA .

⁸School of Physics, University of New South Wales, Kensington, Australia.

⁹ARC Centre for Excellence in All-Sky Astrophysics in 3D.

¹⁰International Centre for Radio Astronomy Research, University of Western Australia, 7 Fairway, Crawley, 6009, WA, Australia.

¹¹Universitäts-Sternwarte, Fakultät für Physik, Ludwig-Maximilians-Universität München, Scheinerstr. 1, 81679, München, Germany.

*Corresponding author(s). E-mail(s): kglazebrook@swin.edu.au;

The formation of galaxies by gradual hierarchical co-assembly of baryons and cold dark matter halos is a fundamental paradigm underpinning modern astrophysics[1, 2] and predicts a strong decline in the number of massive galaxies at early cosmic times[3–5]. Extremely massive quiescent galaxies (stellar masses $> 10^{11} M_{\odot}$) have now been observed as early as 1–2 billions years after the Big Bang[6–13]; these are extremely constraining on theoretical models as they form 300–500 Myr earlier and only some models can form massive galaxies this early [12, 14]. Here we report on the spectroscopic observations with the James Webb Space Telescope of a massive quiescent galaxy ZF-UDS-7329 at redshift 3.205 ± 0.005 that eluded deep ground-based spectroscopy[8], is significantly redder than typical and whose spectrum reveals features typical of much older stellar populations. Detailed modelling shows the stellar population formed around 1.5 billion years earlier in time ($z \sim 11$) at an epoch when dark matter halos of sufficient hosting mass have not yet assembled in the standard scenario[4, 5]. This observation may point to the presence of undetected populations of early galaxies and the possibility of significant gaps in our understanding of early stellar populations, galaxy formation and/or the nature of dark matter.

The spectrum of ZF-UDS-7329 taken with the NIRSPEC prism disperser (spectral resolution of 40–350) is shown in (Figure 1) and shows clear absorption features such as the 4000Å break and Mg b 5174Å typical of old > 1 Gyr stellar populations. To quantitatively measure the age we considered a range of approaches. First we fitted a grid of FAST++ parametric star formation history models[8] to the spectrum and photometry (see Methods for details) to derive a stellar mass of $1.24 \pm 0.09 \times 10^{11} M_{\odot}$ (consistent with the photometric estimate from reference[8]; hereafter S18), stellar metallicity [Fe/H] of 0.021 ± 0.005 , and an age t_{50} (defined as when 50% of the stellar mass had formed). We find $t_{50} = 1.52 \pm 0.16$ Gyr which is significantly older than other quiescent galaxies at this epoch[6–13]. This accords with the visual presence of the 4000Å break, which only develops in stellar populations at ages $\gtrsim 800$ Myr as illustrated in Figure 2. The spectrum is clearly different, even at our relatively low spectral resolution ($R = 51$ at the break), from younger coeval post-starbursts which show a broader Balmer 3640Å break and strong Balmer absorption lines. This can be seen by the direct comparison in Figure 1 with the well studied[7, 8] $z = 3.717$ post-starburst quiescent galaxy ZF-COS-20115. The fitted dust attenuation is small (< 0.3 mags in the rest frame V -band); we note our sub-mm observations of other objects in the S18 sample have also found low dust and gas content[15]. NIRCAM JWST images of ZF-UDS-7329 reveal a compact, edge-on red disk (effective radius 1.15 ± 0.08 kpc at rest frame $1\mu\text{m}$) that show no evidence for any younger star-forming clumps.

The old age implies a formation at $z \sim 11$ and large volume simulations show that single galaxies of this mass have not yet formed at this time[16]. To understand the potential systematic errors we also fit the spectrum using the code Prospector[17] that has an alternative set of stellar tracks and spectral libraries. This allows us to explore non-parametric star-formation histories which is important as it is possible for parametric histories to misestimate the mass-weighted ages of galaxies[18–20].

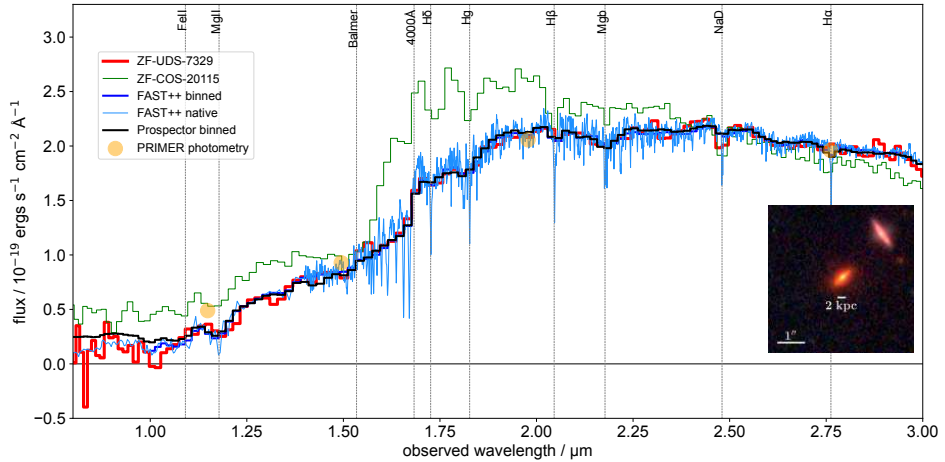


Fig. 1: The JWST NIRSpec spectrum of galaxy ZF-UDS-7329. This covers rest frame 0.2–0.7 μ m and is compared to the best fit FAST++ model which is shown binned to the varying pixel size and resolution of the PRISM spectrum as well as at its original native resolution. Wavelengths of common absorption and emission lines are marked. It can be seen that the 4000 \AA break is well developed and the spectrum is dominated by old cool stellar features. The Prospector fit is very similar. For comparison our recent NIRSpec spectrum of ZF-COS-20115 which has a very similar stellar mass is shown (corrected to the same redshift), this galaxy has been well studied and is significantly younger[7, 8] being quenched for \sim 500 Myr. Its spectrum is more typical of post-starburst quiescent galaxies at this epoch showing a bluer break due to the Balmer limit and strong Balmer absorption lines from hot A stars that remain in the spectrum at this younger age. The PRIMER photometry is also shown and the inset shows the PRIMER image (colour composite of F115W, F200W, and F444W covering rest frame optical bands) Note the spectral and photometric errors from noise are too small to plot in this figure.

Prospector gives a consistent stellar mass, metallicity and low attenuation. We show the reconstruction of the star formation history (SFH) from both codes in Figure 3 with associated uncertainties inferred by Monte Carlo quantiles in each time bin. Both are consistent with old ages with the galaxy forming over 200–400 Myr and all star formation ceasing 1 Gyr before the epoch of observation; Prospector prefers even older populations (up to 1.8 Gyr). Our modelling includes a range of stellar metallicity up to [Fe/H]=0.05; these supersolar values are seen in some objects at these redshifts[10] and due to approximate age-metallicity degeneracies could produce younger age solutions. For our spectrum [Fe/H]=0.05 is excluded as a poor fit at 98% confidence, nevertheless if we force this value in our fitting we still need minimum ages $t_{50} \sim 1$ Gyr. This fit is able to reproduce the overall red colour of the spectrum; however it

differs in the detailed reproductions of the spectral features across the range $1\text{--}3\mu\text{m}$. It can be seen in Figure 2 that high metallicity populations exhibit a different shape around the 4000\AA break due to the increase Fe absorption.

Can such a massive galaxy theoretically be formed at $z \sim 11$? The details of galaxy formation within dark matter halos is complex, but a boundary condition can be placed[4] as the most massive halos have a strongly declining abundance with redshift. Simulations show that haloes with masses $> 10^{11} M_\odot$ closely track the universal cosmic baryon fraction[22] of 16% at $z > 2$; this is lowered by feedback but only at late times and low masses.[23]. We assume this tracking and further assume 100% conversion of halo baryons in to stars could be achievable[4] to calculate a minimum halo mass. We also compare with a 30% conversion which is about the maximum baryon-to-stellar conversion efficiency at $3 < z < 4$ according to semi-empirical estimates of the stellar-halo mass relation[24]; this gives a higher halo mass. For this comparison we need to use the *formed* stellar mass, which is higher than the observed residual stellar mass by 0.17–0.22 dex in our fits; we adopt a formed stellar mass of $2.5 \times 10^{11} M_\odot$ for this comparison. First we use an analytic model [25] to compute the halo mass function as function of redshift; secondly we directly compute the halo mass function from the FLAMINGO Gpc³ simulation[26]. We can approximate the space density of galaxies like ZF-UDS-7329 by dividing the quoted space density in S18 by 24 (for 1 in 24 objects), this gives $6 \times 10^{-7} \text{ Mpc}^{-3}$. This comparison is shown in Figure 3 where we compare the lookback times when the stars form in ZF-UDS-7329 with when halos of suitable mass and number density assemble. It can be seen that this does not occur until $z \sim 6$. To reconcile this we need to have a significant fraction of the stars form more recently than 1 Gyr; however this is excluded by the old age and star-formation history fits.

We can also compare with the actual stellar mass of objects formed in simulations. In the THESAN reionisation simulations[27] of cubic side length 95.5 comoving Mpc, the stellar mass function at $z = 10$ extends to $10^9 M_\odot$ at most with a corresponding space density of 10^{-5} Mpc^{-3} such galaxies. In the MillenniumTNG simulation [16] (740 Mpc side), the highest stellar mass of a galaxy at $z = 11$ is just shy of $10^{10} M_\odot$. If direct ancestors of ZF-UDS-7329 existed in these simulations there would be ~ 200 in this volume.

We next consider other possible systematic errors and erroneous assumptions. Our spectral fitting procedure for the stellar ages marginalises over a broad range of star formation histories, including younger burst populations, and the latter are heavily excluded in all viable fits. In ZF-UDS-7329 there is no evidence for any strong emission lines such as might be associated with non-stellar sources such as Active Galactic Nuclei or residual star-formation. It is significant that even with very high signal:noise ratio (SNR) of 50–70 across the rest-frame optical we are able to obtain a reduced $\chi^2 \sim 2$ with the fits reproducing all the spectral variations. As noted before a high-metallicity solution $[\text{Fe}/\text{H}] = 0.05$ is formally a poor fit; even then this brings t_{50} down to 1 Gyr ($z \sim 6$) which still requires a 100% baryon conversion efficiency that has not been seen in any galaxy. We have assumed a conventional Chabrier Initial Mass Function (IMF); there is some evidence for IMF evolution in $z > 3$ quiescent galaxies but the effect is at most a factor of two lower in stellar mass[28, 29] which is not enough

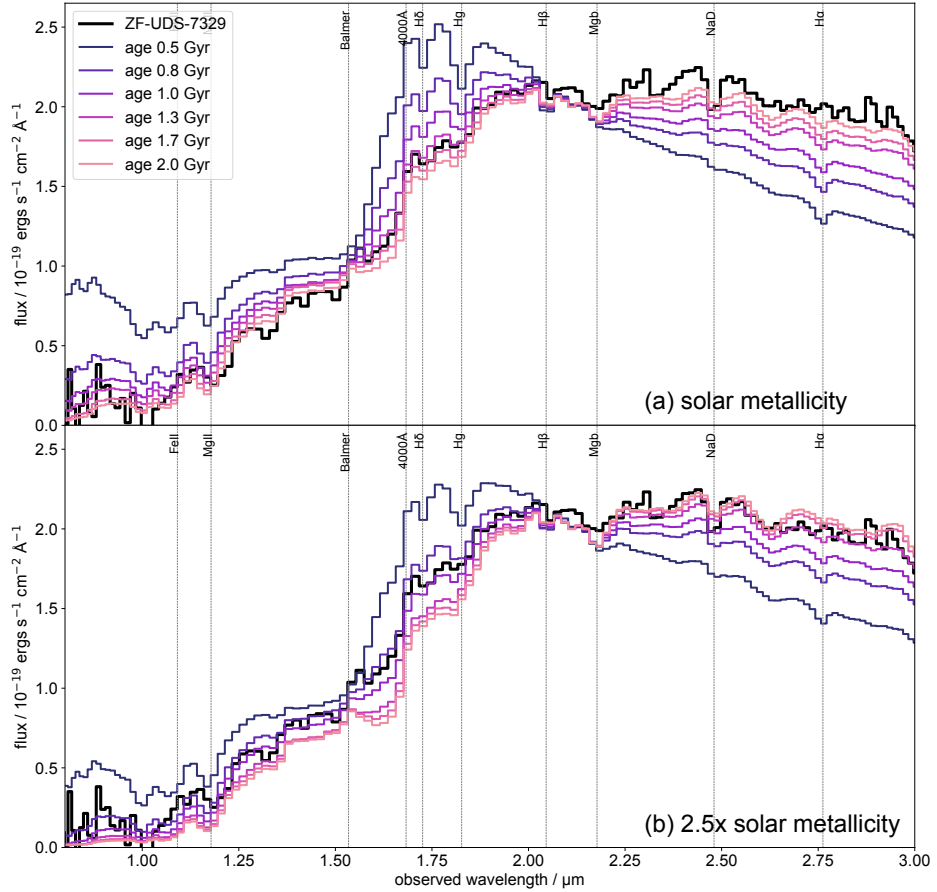


Fig. 2: The effect of age and metallicity on stellar populations. Simple Stellar Population models [21] are compared with the JWST spectrum of ZF-UDS-7329. It can be seen how the transition from a post-starburst type spectrum with a Balmer break and Balmer lines from young A stars to an evolved population with a 4000Å break happens at > 800 Myr. Panel (a) shows how the model at $\simeq 1.7$ Gyr is an excellent match to the data for solar metallicity $[\text{Fe}/\text{H}] = 0$. It can be seen how the strong Balmer lines disappear. Panel (b) shows supersolar metallicity $[\text{Fe}/\text{H}] = 0.05$. As expected due to age–metallicity degeneracy the overall shape best matches at a younger age ($\simeq 1.0$ Gyr); however the detailed features of the spectrum are not well reproduced particularly around the 4000Å break, this is expected as this feature is produced by numerous metal absorption lines. Overall the rest frame optical spectrum is not consistent with a supersolar model.

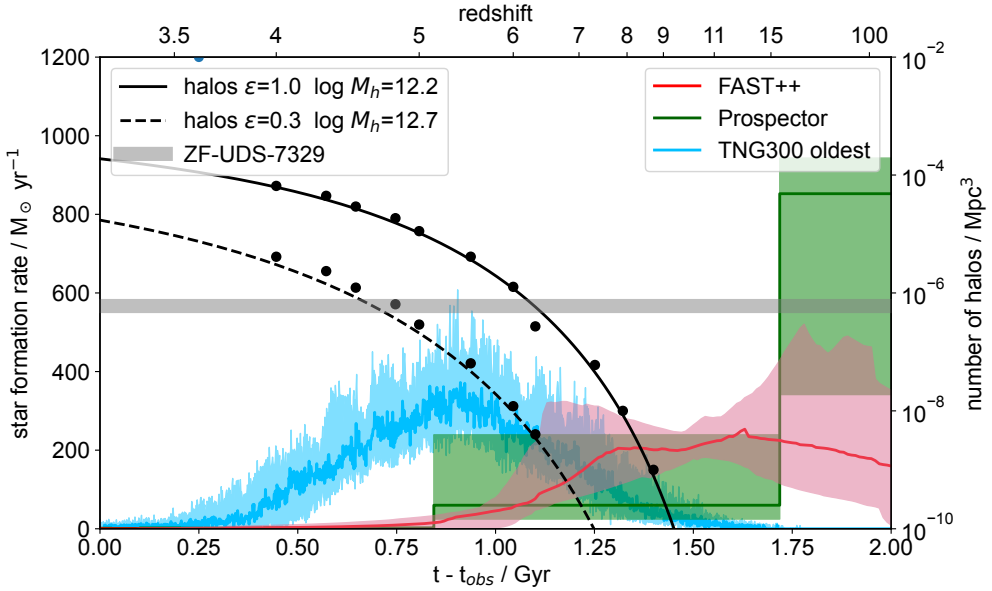


Fig. 3: Comparison of star formation histories with dark matter halo assembly histories. The red and green lines represent FAST++ and Prospector star formation histories inferred from our fitting to ZF-UDS-7329 with the shading showing 16 and 84 percentile ranges in each time bin derived from our Monte Carlo procedure. The FAST++ fits are of dual exponential functional form whereas the Prospector ones are stepwise. Both modelling procedures, utilising different spectral libraries and codes, produce broadly similar star formation histories peaked towards very old ages with the majority of the stars forming at ages $\gtrsim 1.5$ Gyr. The blue band shows the median star formation history (with 16/84 percentiles) of the 20 oldest massive quiescent galaxies in TNG300 at $z = 3$ for comparison. The evolving density of massive cold dark matter halos calculated analytically are shown as solid and dashed black lines for two different halo masses set by two choices of baryon conversion efficiency. The round circles show the $z > 4$ results from the FLAMINGO simulation for the same masses. The estimated space density derived from this galaxy is shown as a horizontal grey band.

to make a significant difference to our conclusions. A more exotic IMF assumption could drastically lower the inferred stellar masses and there could be other issues such as large mismatches between local templates and early stellar populations.

In Λ CDM formation models the prediction is that such a galaxy would have to build up from numerous mergers in its recent past; however this still predicts young ages as star formation tracks halo growth. We quantitatively test the limit of the theoretical expectation by selecting 283 quiescent galaxies from the Illustris TNG300 simulation[30] with stellar mass $> 10^{10.8} M_\odot$ and specific star formation rate < 0.15 Gyr^{-1} (following S18) and tracing their star formation histories through their halo progenitor trees. Additionally we compute t_{50} for each galaxy and select the 20 oldest

ones; this approximates the number density of ZF-UDS-7329 and our pre-selection of the oldest object. We show the median star formation history of these 20 objects in Figure 3; even with this extreme assumption we find $t_{50} = 890 \pm 50$ Myr with a significant amount of star formation younger than 1 Gyr; which is a marked contrast to our galaxy. The halo mass growth follows a similar trajectory.

Finally we could consider if more exotic cosmological models can produce massive halos earlier in cosmic history. Though there is no obvious alternative to vanilla cold dark matter which would clearly do this we note that exotic dark matter models can exert a strong influence on early galaxy formation formation [31, 32]. However these do not necessarily go in the right direction, for example popular Warm Dark Matter models suppress the abundance of lower mass galaxies but make little difference at the high-mass end[33]. Modifying the initial power spectrum by introducing a ‘blue tilt’ would be one potential solution[34, 35] as is ‘Early Dark Energy’[5] or early seeds from massive primordial black holes[36].

The apparent formation of ZF-UDS-7329 at such an early epoch points to significant problems with our current paradigms of early stellar populations and of galaxy formation. It may even violate the basic constrain of their being sufficiently massive dark matter halos. We would speculate that some combination of multiple of these effects is likely responsible. Purely empirically this picture of rapid and early galaxy formation is consistent with the direction of other early results from JWST such as the unexpected overabundance of very luminous $10 < z < 12$ star-forming galaxies, identified photometrically, compared to simulations[26]. Many of these are now spectroscopically confirmed[37, 38] though we note their stellar masses extremely uncertain and very bursty star-formation may be an alternative explanation of the UV luminosity function[39]. There is also the photometric identification of six candidate star forming galaxies with high stellar mass ($\sim 10^{10} M_\odot$) [40] at $7 < z < 9$. This comparison is particularly interesting as these candidates also stress basic halo mass constraints[5]; however they have yet to be spectroscopically confirmed except for two galaxies which turned out to be significantly lower mass.[38] ZF-UDS-7329 is 60% more massive than the most massive candidate in that sample (and a factor of 9 more massive than the median). A plausible scenario could be constructed in which these are a population of ancestors that merge to make galaxies like ZF-UDS-7329.

We have presented a galaxy at $z = 3.205$ whose very old age, rapid formation and extreme stellar mass are difficult to reconcile with current paradigms of early galaxy formation; these may require significant revision. The main limitation of this work is of course the inferences are based on the discovery of a single object. The inferred sky density is only of order 8 deg^{-2} at $3 < z < 4$ so they are a rare class of source. The next step is the photometric discovery of more such galaxies to be certain of their abundance, and higher spectral resolution observations to measure more constraining elemental abundances and stellar ages. Fortunately both of these are well within the capability of JWST[41]; if their existence is a challenge to the Λ CDM galaxy formation paradigm this will be resolved definitively soon.

Acknowledgments. K.G. thanks Roberto Abraham for assistance in fetching data on $z = 0$ comparison galaxies from Canadian archives and Jarle Brinchmann for

inspiring discussions on the $0.94\mu\text{m}$ bump. This work is based on observations made with the NASA/ESA/CSA James Webb Space Telescope. The data were obtained from the Mikulski Archive for Space Telescopes at the Space Telescope Science Institute, which is operated by the Association of Universities for Research in Astronomy, Inc., under NASA contract NAS 5-03127 for JWST. These observations are associated with program 2565. We thank all the hard work of the JWST team which made this great observatory possible. We thank Michael Maseda and Allison Strom for helpful discussions during the data reduction process. T.N., K. G., and C.J. acknowledge support from Australian Research Council Laureate Fellowship FL180100060. This work has benefited from funding from the Australian Research Council Centre of Excellence for All Sky Astrophysics in 3 Dimensions (ASTRO 3D), through project number CE170100013. C.P. acknowledges generous support from Marsha L. and Ralph F. Schilling and from the George P. And Cynthia Woods Mitchell Institute for Fundamental Physics and Astronomy. The Cosmic Dawn Center is funded by the Danish National Research Foundation (DNRF) under grant DNRF140. P.O. is supported by the Swiss National Science Foundation through project grant 200020_207349. This work received funding from the Swiss State Secretariat for Education, Research and Innovation (SERI).

Author Contributions. K.G. did all the final data analysis, made the figures and wrote the manuscript. T.N. reduced the NIRSpec data and ran FAST++ and Prospector model fits. C.S. originally identified ZF-UDS-7329 as an interesting object in S18 and analysed deep ground based spectra that failed to secure a redshift but motivated the JWST program. C.S. also added the LSF functionality to FAST++ and `slinefit` codes for this paper. C.L. and A.C-G. provided the comparisons with halos in simulations. L.K. processed the NIRCam data. H.C. did TNG300 and THESAN comparisons. All other authors contributed to the scientific discussions in the proposal and manuscript.

Data Availability. We make the full JWST spectrum of ZF-UDS-7329 and associated Line Spread Function available in the CSV format small file `final_spectrum_pub.csv`. This is the Source Data for Figures 1, 2 and Extended Data Figure 2. The photometry is given in Extended Table 1. The wavelength units are in μm (observed frame) and the flux units are in $10^{-19} \text{ ergs cm}^{-2} \text{ s}^{-1} \text{ \AA}^{-2} \text{ s}^{-1}$.

Code Availability. All software packages used in this analysis are publicly available. In particular FAST++, Prospector- α and the `hmf` python module are available on GitHub.

References

- [1] Blumenthal, G. R., Faber, S. M., Primack, J. R. & Rees, M. J. Formation of galaxies and large-scale structure with cold dark matter. *Nature* **311**, 517 – 525 (1984).
- [2] Somerville, R. S. & Davé, R. Physical Models of Galaxy Formation in a Cosmological Framework. *Ann. Rev. Astron. Astrophys.* **53**, 51–113 (2015).

- [3] Glazebrook, K. *et al.* A high abundance of massive galaxies 3-6 billion years after the Big Bang. *Nature* **430**, 181 – 184 (2004).
- [4] Behroozi, P. & Silk, J. The most massive galaxies and black holes allowed by Λ CDM. *Mon. Not. R. Astron. Soc.* **477**, 5382 – 5387 (2018).
- [5] Boylan-Kolchin, M. Stress testing Λ CDM with high-redshift galaxy candidates. *Nature Astronomy* **7**, 731–735 (2023).
- [6] Marsan, Z. C. *et al.* Spectroscopic Confirmation of an Ultra Massive and Compact Galaxy at $z = 3.35$: a Detailed Look at an Early Progenitor of Local Giant Ellipticals. *Astrophys. J.* **801**, 133 (2015).
- [7] Glazebrook, K. *et al.* A massive, quiescent galaxy at a redshift of 3.717. *Nature* **544**, 71–74 (2017).
- [8] Schreiber, C. *et al.* Jekyll & Hyde: quiescence and extreme obscuration in a pair of massive galaxies 1.5 Gyr after the Big Bang. *Astron. Astrophys.* **611**, A22 (2018).
- [9] Forrest, B. *et al.* An Extremely Massive Quiescent Galaxy at $z = 3.493$: Evidence of Insufficiently Rapid Quenching Mechanisms in Theoretical Models. *Astrophys. J. Lett.* **890**, L1 (2020).
- [10] Saracco, P. *et al.* The Rapid Buildup of Massive Early-type Galaxies: Supersolar Metallicity, High Velocity Dispersion, and Young Age for an Early-type Galaxy at $z = 3.35$. *Astrophys. J.* **905**, 40 (2020).
- [11] Forrest, B. *et al.* The Massive Ancient Galaxies at $z > 3$ NEar-infrared (MAGAZ3NE) Survey: Confirmation of Extremely Rapid Star Formation and Quenching Timescales for Massive Galaxies in the Early Universe. *Astrophys. J.* **903**, 47 (2020).
- [12] Valentino, F. *et al.* Quiescent Galaxies 1.5 Billion Years after the Big Bang and Their Progenitors. *Astrophys. J.* **889**, 93 (2020).
- [13] Antwi-Danso, J. *et al.* The FENIKS Survey: Spectroscopic Confirmation of Massive Quiescent Galaxies at $z \sim 3$ –5. *arXiv e-prints* arXiv:2307.09590 (2023).
- [14] Merlin, E. *et al.* Red and dead CANDELS: massive passive galaxies at the dawn of the universe. *Mon. Not. R. Astron. Soc.* **490**, 3309–3328 (2019).
- [15] Suzuki, T. L. *et al.* Low Star Formation Activity and Low Gas Content of Quiescent Galaxies at $z = 3.5$ –4.0 Constrained with ALMA. *Astrophys. J.* **936**, 61 (2022).
- [16] Kannan, R. *et al.* The MillenniumTNG project: The galaxy population at $z \geq 8$. *Mon. Not. R. Astron. Soc.* **524**, 2594–2605 (2023).

- [17] Johnson, B. D., Leja, J., Conroy, C. & Speagle, J. S. Stellar Population Inference with Prospector. *Astrophys. J. Supp.* **254**, 22 (2021).
- [18] Carnall, A. C. *et al.* How to Measure Galaxy Star Formation Histories. I. Parametric Models. *Astrophys. J.* **873**, 44 (2019).
- [19] Leja, J. *et al.* A New Census of the $0.2 < z < 3.0$ Universe. I. The Stellar Mass Function. *Astrophys. J.* **893**, 111 (2020).
- [20] Suess, K. A. *et al.* Recovering the Star Formation Histories of Recently Quenched Galaxies: The Impact of Model and Prior Choices. *Astrophys. J.* **935**, 146 (2022).
- [21] Bruzual, G. & Charlot, S. Stellar population synthesis at the resolution of 2003. *Mon. Not. R. Astron. Soc.* **344**, 1000–1028 (2003).
- [22] Ayromlou, M., Nelson, D. & Pillepich, A. Feedback reshapes the baryon distribution within haloes, in halo outskirts, and beyond: the closure radius from dwarfs to massive clusters. *Mon. Not. R. Astron. Soc.* **524**, 5391–5410 (2023).
- [23] Wright, R. J., Lagos, C. d. P., Power, C. & Mitchell, P. D. The impact of stellar and AGN feedback on halo-scale baryonic and dark matter accretion in the EAGLE simulations. *Mon. Not. R. Astron. Soc.* **498**, 1668–1692 (2020).
- [24] Behroozi, P., Wechsler, R. H., Hearn, A. P. & Conroy, C. UniverseMachine: The correlation between galaxy growth and dark matter halo assembly from $z = 0\text{--}10$. *Mon. Not. R. Astron. Soc.* **488**, 3143–3194 (2019).
- [25] Reed, D. S., Bower, R., Frenk, C. S., Jenkins, A. & Theuns, T. The halo mass function from the dark ages through the present day. *Mon. Not. R. Astron. Soc.* **374**, 2 – 15 (2007).
- [26] Schaye, J. *et al.* The FLAMINGO project: cosmological hydrodynamical simulations for large-scale structure and galaxy cluster surveys. *Mon. Not. R. Astron. Soc.* **526**, 4978–5020 (2023).
- [27] Kannan, R. *et al.* Introducing the THESAN project: radiation-magnetohydrodynamic simulations of the epoch of reionization. *Mon. Not. R. Astron. Soc.* **511**, 4005–4030 (2021).
- [28] Esdaile, J. *et al.* Consistent Dynamical and Stellar Masses with Potential Light IMF in Massive Quiescent Galaxies at $3 < z < 4$ Using Velocity Dispersions Measurements with MOSFIRE. *Astrophys. J. Lett.* **908**, L35 (2021).
- [29] Forrest, B. *et al.* MAGAZ3NE: High Stellar Velocity Dispersions for Ultramassive Quiescent Galaxies at $z \geq 3$. *Astrophys. J.* **938**, 109 (2022).
- [30] Nelson, D. *et al.* The IllustrisTNG Simulations: Public Data Release. *Computational Astrophysics & Cosmology* **6**, 2 (2019).

- [31] Dayal, P., Mesinger, A. & Pacucci, F. Early Galaxy Formation in Warm Dark Matter Cosmologies. *Astrophys. J.* **806**, 67 (2015).
- [32] Maio, U. & Viel, M. JWST high-redshift galaxy constraints on warm and cold dark matter models. *Astronomy & Astrophysics* **672**, A71 (2023).
- [33] Lin, H., Gong, Y., Yue, B. & Chen, X. Implications of the Stellar Mass Density of High-z Massive Galaxies from JWST on Warm Dark Matter. *arXiv e-prints* arXiv:2306.05648 (2023).
- [34] Parashari, P. & Laha, R. Primordial power spectrum in light of JWST observations of high redshift galaxies. *Mon. Not. R. Astron. Soc.* **526**, L63–L69 (2023).
- [35] Padmanabhan, H. & Loeb, A. Alleviating the Need for Exponential Evolution of JWST Galaxies in $10^{10} M_{\odot}$ Haloes at $z > 10$ by a Modified Λ CDM Power Spectrum. *Astrophys. J. Lett.* **953**, L4 (2023).
- [36] Liu, B. & Bromm, V. Accelerating Early Massive Galaxy Formation with Primordial Black Holes. *Astrophys. J. Lett.* **937**, L30 (2022).
- [37] Curtis-Lake, E. *et al.* Spectroscopic confirmation of four metal-poor galaxies at $z = 10.3\text{--}13.2$. *Nature Astronomy* **7**, 622–632 (2023).
- [38] Fujimoto, S. *et al.* CEERS Spectroscopic Confirmation of NIRCam-selected $z \geq 8$ Galaxy Candidates with JWST/NIRSpec: Initial Characterization of Their Properties. *Astrophys. J. Lett.* **949**, L25 (2023).
- [39] Sun, G. *et al.* Bursty Star Formation Naturally Explains the Abundance of Bright Galaxies at Cosmic Dawn. *Astrophys. J. Lett.* **955**, L35 (2023).
- [40] Labb  , I. *et al.* A population of red candidate massive galaxies 600 Myr after the Big Bang. *Nature* **616**, 266–269 (2023).
- [41] Carnall, A. C. *et al.* A massive quiescent galaxy at redshift 4.658. *Nature* **619**, 716–719 (2023).
- [42] Mason, R. E. *et al.* The Nuclear Near-Infrared Spectral Properties of Nearby Galaxies. *Astrophys. J. Supp.* **217**, 13 (2015).

Methods

NIRSPEC data reduction and calibration

We observed the galaxy ZF-UDS-7329 with JWST on August 1st 2022 using the NIRSpec instrument in the MSA mode [43] as part of our program #2565 whose goal was to secure spectroscopic redshifts of all objects in S18 which eluded deep ground-based spectroscopy. The PRISM disperser was used producing spectra covering the wavelength range 0.6–5.0 μ m at a spectral resolution ranging from 40 to 350 from blue to red ends. The galaxy was observed in three dither positions using a 5-shutter nod pattern (which has a nod distance large enough to avoid self-subtraction) and was close to centred transversely in the slit. We reduced the data to 2D flux calibrated spectra using the STScI pipeline v1.12.5 with CRDS context `jwst_1152.pmap` and used MSAEXP v0.6.18 to extract the 2D to 1D spectra.

Absolute spectrophotometric calibration of NIRSPEC data is difficult due to the narrow 0.2 arcsec slit and the wavelength-dependent point spread function (PSF) that causes significant additional aperture loss. Our calibration strategy was as follows: first we wished to verify that the spectrophotometry *through the slit* agreed with NIRCAM photometry of the same galaxy. To do this we reduced the data in the pipeline’s ‘point source calibration mode’ but remove the `pathloss` step that corrects for de-centering and point sources and instead manually apply the *uniform* pathloss correction. Because of the software definitions of these quantities ([44], p.10) the effect of this is to remove the point source aperture correction and return the flux through the slit. This we can then compare using synthetic slit photometry on NIRCAM images; because the PSF is dominated by the telescope it will be very similar in NIRCAM and NIRSPEC. This comparison is showing in Extended Data Figure 1 and it is excellent with a median offset of 0.13 mags and an RMS residual of ~ 0.03 mags. (We expect small differences as the PSF would not be exactly the same and there will be small pointing errors). Given this validation of the slit calibration we next correct for aperture loss by fitting a second order polynomial to the ratio of the total NIRCAM photometry to the slit photometry. In general we expect a wavelength dependence at this step as the slit photometry now includes PSF aperture losses; however because the source is very uniform in colour and resolved this is only a small effect. We use the F150W–F277W colour which straddles the 4000 \AA break to quantify this, correcting to total makes the colour 0.1 mags bluer which makes the spectral age younger, not older.

Finally we validated the formal propagation of uncertainties in the pipeline. We did this by comparing the individual spectra at the 3 dither positions and computing the RMS between them vs wavelength (after photometrically calibrating them to have the same overall shape). We expect on average this to approximately equal $\sqrt{2} \times$ the uncertainty, and we do indeed find this broad agreement; noting this is a noisy comparison as there are a large number of outliers on single dither spectra due to defects or cosmic rays in individual exposures. We also find excellent χ^2 in the fitting when using the pipeline uncertainties which supports the noise model being correct.

ZF-COS-20115[7, 8] was also re-observed with JWST as a MSA filler in our program; the spectrum was reduced and calibrated using an identical procedure and

serves as a useful comparison for the more typical $3 < z < 4$ post-starburst massive quiescent galaxy.

NIRCam analysis

NIRCAM images were taken as part of the PRIMER survey (program GO #1837); we used the reductions and global photometry from the DAWN JWST archive[45] v6 data release in a 0.7 arcsec diameter aperture. We provide the NIRCAM photometry in Extended Data Table 1.

To measure the object size we perform two-dimensional fits to the surface brightness distributions of the NIRCam F444W galaxy images using a Python package, `Galight` [46]. With `Galight`, we prepare a cutout galaxy image, detect neighboring sources in the field of view; `Galight` allows for simultaneously fitting of as many neighboring objects as needed, in order to avoid source blending. We fit a single-component Sérsic profiles to the two dimensional surface brightness distributions of all detected objects, making use of galaxy imaging data, the noise level maps, and custom-made PSF models. The fit parameters are total magnitudes (M), half-light radius (r_e), Sérsic index (n), and axis ratio (b/a). With the input ingredients, `Galight` convolves the theoretical models (i.e., Sérsic profile) with the Point Spread Function (PSF) before fitting them to the galaxy images. We define the effective radius as the semi-major axis of the ellipse that contains half of the total flux of the best-fitting Sérsic model. We find the effective radius to be $r_e = 1.15^{+0.08}_{-0.08}$ kpc, the Sérsic index to be $n = 2.41^{+0.24}_{-0.29}$ and the axis ratio (b/a) = $0.33^{+0.01}_{-0.01}$ — all consistent with the visual appearance of an edge on disk which is shown in Figure 1.

Spectroscopic Line Spread Function

The NIRSpec PRISM disperser has a very low and non-linear spectral resolution and dispersion scale. This coupled with the high SNR per pixel of the spectrum makes it quite important to account for systematic errors in the fitting. In particular the wavelength-dependent line spread function (LSF) is significant and without accounting for this we can not obtain acceptable fits, especially around the 4000Å break. To calculate the LSF we first need a model for the image size, as the galaxy is smaller than the slit width. This we obtain from the PRIMER images (which has very closely the same PSF as the NIRSpec focal plane), we supersample them and project them along the slit to obtain a 1D profile across the slit in each band. We find these projected profiles are well approximated by a gaussian function with a small and smooth increase in effective image size from 0.16 to 0.18 arcsec (Full Width Half Maximum) with wavelength due to the telescope's diffraction. This increase is well approximated by a linear function. Multiplying this by the PRISM dispersion function[47] gives the LSF width as a function of wavelength.

Spectroscopic redshift determination

We use `slinefit` (S18) which fits stellar and emission line templates, We use version 2.3 where we added the feature to include a wavelength dependent LSF in the modelling. We obtain a redshift of $z = 3.205 \pm 0.005$ and a template fit very similar to those

we found later with full stellar population modelling. We derived this redshift error using Monte Carlo simulations taking a 1.5 Gyr old Bruzual & Charlot 2003 ‘Simple Stellar Population’ model[21], which approximates the spectrum of our galaxy, varying the redshift from 3.19 to 3.23 and creating simulated NIRSPEC spectra including LSF and pixelisation. We find the typical redshift recovery with `slinefit` is ± 0.005 over this range; which is about $\pm 1/8$ th of a spectral pixel at $2\mu\text{m}$ which seems reasonable for high SNR full spectrum fitting. The accuracy gets considerably worse if the LSF is ignored. We also estimate the effect of the redshift error on the spectral modelling which is a potential concern given our high SNR but coarse resolution. We do this by shifting and re-simulating the model; we find a redshift error of 0.01 introduces systematic flux residuals at the 1% level which is below that of our other noise sources.

FAST++ and Prospector fitting

We use FAST++ version 1.5.0 which was enhanced by us to include a wavelength dependent LSF in the modelling. The spectral libraries used by FAST++ are only well characterised at spectroscopic resolution in the rest-frame optical; therefore we limit the fitting to rest frame wavelengths $< 0.8\mu\text{m}$. We use the same general star formation history (SFH) models as S18 and identical parameter ranges (as listed S18 Table 1); modelling the SFH as an exponential rise and fall at earlier times plus a component of recent residual star formation. The latter is often useful when there is a superposition of old and young stellar populations which can bias mass and age estimates; however we find the young component is negligible in the case of ZF-UDS-7329. We allow metallicity to vary up to $2.5 \times$ solar and adopt a Chabrier Initial Mass Function[48]. The underlying models utilise standard solar-scaled element abundances. Burst times are allowed to go as short as 10 Myr which can be important for unbiased estimates of quenching rates[20]. For each model evaluation we compute the time at which 50% of the stars had formed for the trial set of parameters. We marginalise over the model grid and determine errors on model parameters, derived parameters and on the SFH at that time step using 1000 Monte-Carlo simulations.

For Prospector we use the same LSF model as for FAST++. We corrected an issue in the interpolation of the high-resolution spectral models which caused incorrect pixel downsampling to our low spectral resolution.[49] Our version is provided in a GitHub fork [50]. We limit fitting to rest frame wavelengths $< 0.7\mu\text{m}$; as recommended for these stellar libraries according to the Prospector documentation. We use a `continuity_sfh` to model the formation history of our galaxy[51] with 7 custom time bins. These follow the default approximately logarithmic sampling at young ages, important for capturing potential recent star formation, but we impose finer sampling of 0.25 Gyr at ages > 1 Gyr to capture the epoch of maximum star formation more carefully. We additionally let the stellar metallicity ($-2 \leq \log_{10}(Z/Z_\odot) \leq 0.19$) and the dust optical depth ($0 \leq \tau \leq 2.0$) vary as free parameters. Our bins are fixed in time; simulations have shown that this choice[20] can accurately recover ages but have difficulty recovering the duration of recent quenching episodes due to rounding errors at bin edges; however our quenching proves not to be recent and we are not trying to accurately resolve in time the quenching event. Higher spectral resolution data would

allow more flexible models to be explored. As shown in the main text given our choices we find strong agreement between parametric and non-parametric approaches.

Since we do explicit calibration of the data to the photometry, we do not consider the similar options in FAST++ and Prospector that allow an extra polynomial function to be fitted to do this. In both cases we include the 1–5 μm PRIMER photometry in the fits though this makes little practical difference as the weights are dominated by very high SNR spectrum.

For both codes we find reduced $\chi^2 \sim 2$ in the best fits which is excellent given there are ~ 100 independent spectral pixels each with SNR of 50–70. (The models have 7–9 free parameters.) The χ^2 gets much worse if we do not include the LSF in the fit or do the downsampling incorrectly.

Extended Data Figure 3 shows the effect of force fitting the [Fe/H]=0.05 solution which is formally excluded. As expected the age can come down to ~ 1 Gyr but a substantial amount of star formation is still preferred at ages > 1.3 Gyr and the age distribution of star formation remains significantly older than in the TNG300 galaxies. There is more disagreement between FAST++ and Prospector which we attribute to the effect of the mismatch of the supersolar model to the spectrum.

Rest frame near-infrared spectrum

Our model fitting excludes rest-frame wavelengths $> 0.8\mu\text{m}$ as the stellar libraries that underpin the models are currently poorly determined in this region. We show this wavelength range in Extended Data Figure 2. The extrapolation of the best fitting Prospector model is overlaid on the figure; though it reproduces the overall spectral shape the detailed spectral variations are not reproduced.

However we can still see if the spectrum in this wavelength range is qualitatively consistent with an old population by comparing empirically with nearby galaxy templates. We do indeed notice several features consistent with the presence of older stellar populations. Most noticeable is the broad absorption bump at 0.94 μm . This feature is known, but not well represented in stellar libraries, as at $z = 0$ the wavelength range overlaps with significant telluric absorption [52]. It is thought to be due to a mixture of ZrO, CN and TiO features in Thermally Pulsing Asymptotic Giant Branch stars [52]. Empirically this bump appears in stellar populations older than a Gyr.

We compare with low redshift galaxies from [42]. This sample is near-infrared spectra of nearby galaxy nuclei many of which harbour weak Active Galactic Nuclei (AGN) so this is not ideal. We choose two example objects from here that are classified as dominated by old stellar populations and with no AGN emission lines. NGC 205 is an intermediate age (< 1 Gyr) post-starburst; it has a hotter spectrum, and a weaker bump than ZF-UDS-7329. In contrast the spectrum of NGC 5850 (with age ~ 5 Gyr) has a much stronger bump qualitatively similar to what we see. The CN feature at rest frame 1.1 μm demonstrates similar behaviour. Overall the rest-frame near-infrared spectrum of our galaxy is consistent with ages older than a Gyr.

The current lack of coverage of the near-infrared templates is due to the issues of spectroscopy from the ground at wavelengths with significant atmospheric absorption. This situation is likely to improve rapidly due to the capabilities of JWST.

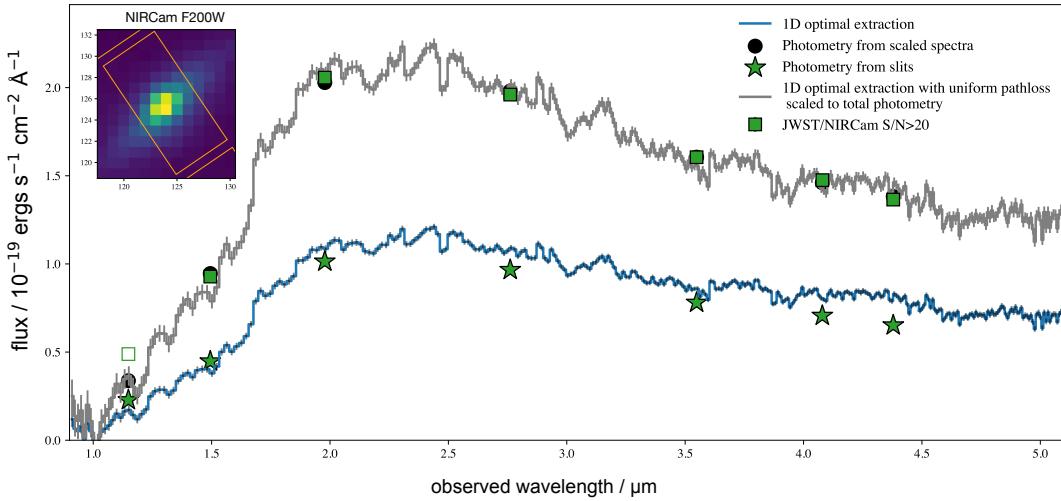
Halo masses

The halo mass functions were computed using the python `hmf` module v3.4.4 which implements a wide variety of analytic predictions. We found that at our high redshifts the resulting mass functions did not vary significantly with choice of model and agreed well with the results from the large volume FLAMINGO simulation.

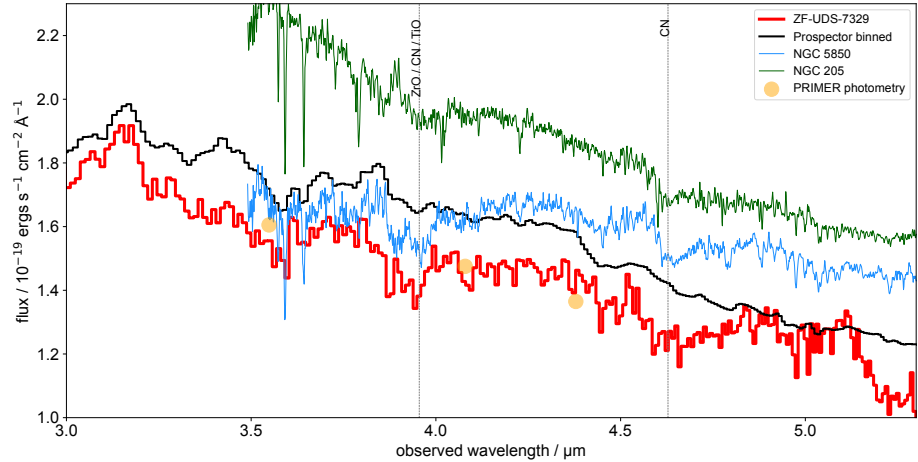
We adopt a cosmology of $\Omega_m = 0.3$, $\Omega_\Lambda = 0.7$, $H_0 = 70 \text{ km}^{-1} \text{ s}^{-1} \text{ Mpc}^{-1}$ for time and halo mass analytic calculations. We note that there is a small difference in FLAMINGO; with the main one being the use of $H_0 = 67 \text{ km}^{-1} \text{ s}^{-1} \text{ Mpc}^{-1}$ but this has negligible impact on the comparison.

Band	mag
F115W	25.567 ± 0.034
F150W	24.299 ± 0.009
F200W	22.826 ± 0.002
F277W	22.154 ± 0.001
F356W	21.827 ± 0.001
F410M	21.616 ± 0.001
F444W	21.546 ± 0.001

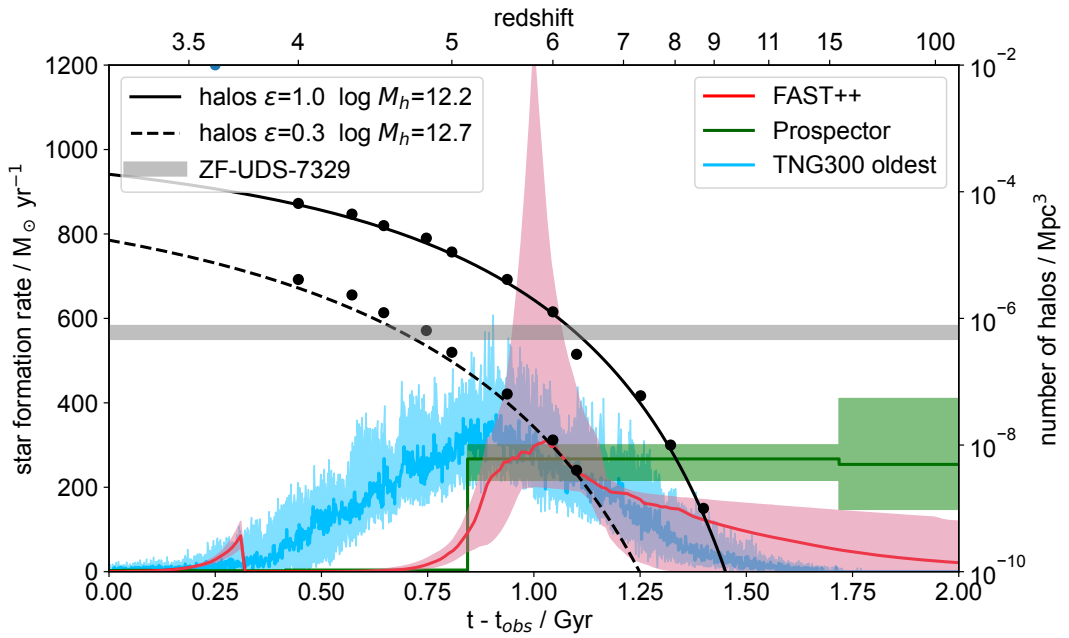
Extended Data Table 1: NIRCam integrated photometry for ZF-UDS-7329. Note the tabulated random errors are small for such a bright galaxy; it is estimated that systematic errors are of order 0.02 mags.[54]



Extended Data Figure 1: Flux calibration of the NIRSpec spectrum. The lower blue curve shows the derived flux through the slit, compared with NIRCAM photometry with a synthetic slit aperture. This shows very good agreement. The upper grey curve shows the correction of the spectrum to total NIRCAM photometry. Both spectra show have flux error bars superimposed. The inset shows the MSA shutter footprint overlaid on the NIRCAM F200W image.



Extended Data Figure 2: Comparison of spectra at longer wavelengths. ZF-UDS-7329 in the rest frame $0.7\text{--}1.3\mu\text{m}$ region is compared to redshifted high signal:noise spectra[42] of the nuclei of local NGC galaxies (these are normalised to the same flux at $0.9\text{--}0.95\mu\text{m}$ rest and then offset for clarity). NGC 5850 is a nearby spiral with a luminosity weighted age of ~ 5 Gyr, and it can be seen that the $0.94\mu\text{m}$ absorption (ZrO, CN, TiO bands) is quite similar, and there is overall a very good match between them to the bumps and wiggles in the continuum which arise from numerous molecular bands in cool stars. NGC205's light is dominated by an intermediate age population ($0.1\text{--}1$ Gyr) and it can be seen that the $0.94\mu\text{m}$ feature, and other molecular bands are much weaker. Note the flux axis is greatly zoomed compared to Figure 1 to highlight very weak absorption features.



Extended Data Figure 3: Comparison of star formation histories with dark matter halo assembly histories for high metal abundance. This is a version of Figure 3 where we force fit the poor fit model with $[Fe/H] = 0.05$. The age is reduced to ~ 1 Gyr but is still significantly discrepant with theoretical expectations. Colours, lines and symbols are as in Figure 3.

Methods References

- [43] Ferruit, P., Jakobsen, P., Giardino, G., Rawle, T., Alves de Oliveira, C., Arribas, S., Beck, T.L., Birkmann, S., Böker, T., Bunker, A.J., Charlot, S., de Marchi, G., Franx, M., Henry, A., Karakla, D., Kassin, S.A., Kumari, N., López-Caniego, M., Lützgendorf, N., Maiolino, R., Manjavacas, E., Marston, A., Moseley, S.H., Muzerolle, J., Pirzkal, N., Rauscher, B., Rix, H.-W., Sabbi, E., Sirianni, M., te Plate, M., Valenti, J., Willott, C.J., Zeidler, P.: The Near-Infrared Spectrograph (NIRSpec) on the James Webb Space Telescope. II. Multi-object spectroscopy (MOS). *Astron. Astrophys.* **661**, 81 (2022)
- [44] Ferruit, P.: The correction of path losses for uniform and point sources. ESA NIRSPEC Technical Note **ESA-JWST-SCI-NRS-TN-2016-017** (2016). https://dms.cosmos.esa.int/COSMOS/doc_fetch.php?id=3520285 [Accessed: 20/Jul/2023]
- [45] Gabriel Brammer: The DAWN JWST Archive. <https://dawn-cph.github.io/dja/>. Accessed: 2023-12-09
- [46] Ding, X., Silverman, J., Treu, T., Schulze, A., Schramm, M., Birrer, S., Park, D., Jahnke, K., Bennert, V.N., Kartaltepe, J.S., Koekemoer, A.M., Malkan, M.A., Sanders, D.: The Mass Relations between Supermassive Black Holes and Their Host Galaxies at $1 < z < 2$ HST-WFC3. *Astrophys. J.* **888**(1), 37 (2020)
- [47] Space Telescope Science Institute: NIRSpec Dispersers and Filters. <https://jwst-docs.stsci.edu/jwst-near-infrared-spectrograph/nirspec-instrumentation/nirspec-dispersers-and-filters>. Accessed: 2023-12-09
- [48] Chabrier, G.: Galactic Stellar and Substellar Initial Mass Function. *Pub. Astron. Soc. Pac.* **115**(8), 763–795 (2003)
- [49] Themiya Nanayakkara: Prospector GitHub Issue 298. <https://github.com/bd-j/prospector/issues/298>. Accessed: 2023-12-09
- [50] Themiya Nanayakkara: Prospector Fork. <https://github.com/themiyan/prospector>. Accessed: 2023-12-09
- [51] Leja, J., Carnall, A.C., Johnson, B.D., Conroy, C., Speagle, J.S.: How to Measure Galaxy Star Formation Histories. II. Nonparametric Models. *Astrophys. J.* **876**(1), 3 (2019) [astro-ph.GA]
- [52] Riffel, R., Mason, R.E., Martins, L.P., Rodríguez-Ardila, A., Ho, L.C., Riffel, R.A., Lira, P., Martin, O.G., Ruschel-Dutra, D., Alonso-Herrero, A., Flohic, H., McDermid, R.M., Almeida, C.R., Thanjavur, K., Winge, C.: The stellar spectral features of nearby galaxies in the near infrared: tracers of thermally pulsing asymptotic giant branch stars? *Mon. Not. R. Astron. Soc.* **450**(3), 3069–3079 (2015)

- [42] Mason, R.E., Rodríguez-Ardila, A., Martins, L., Riffel, R., Martín, O.G., Almeida, C.R., Dutra, D.R., Ho, L.C., Thanjavur, K., Flohic, H., Alonso-Herrero, A., Lira, P., McDermid, R., Riffel, R.A., Schiavon, R.P., Winge, C., Hoenig, M.D., Perlman, E.: The Nuclear Near-Infrared Spectral Properties of Nearby Galaxies. *Astrophys. J. Supp.* **217**(1), 13 (2015)
- [54] Space Telescope Science Institute: JWST Calibration Uncertainties. <https://jwst-docs.stsci.edu/jwst-data-calibration-considerations/jwst-calibration-uncertainties>. Accessed: 2023-12-09

Author Information

The authors declare that they have no competing financial or non-financial interests. Correspondence and requests for materials should be addressed to Karl Glazebrook (kglazebrook@swin.edu.au).

Reprints and permissions information is available at www.nature.com/reprints.